Performance Analysis of Wi-Fi Indoor Localization with Channel State Information

Xiaohua Tian, *Member, IEEE*, Sujie Zhu, Sijie Xiong, Binyao Jiang, Yucheng Yang, and Xinbing Wang, *Senior Member, IEEE*

Abstract—Recently proposed Wi-Fi indoor localization systems utilizing channel state information (CSI) derived from the received signal achieve admirable accuracy. This paper presents an information-theoretical analysis in the received waveform level to explore the fundamental limits of the approach. In particular, we perform frequency domain Cramér-Rao bound (CRB) analysis for location estimation with CSI. Our analysis resolves the high-rank Fisher information matrix challenge, and establishes intrinsic connection between parameters to be estimated for localization and the received waveform information observable with the CSI retrieving toolkit. We also analyze the influence of the asynchronization between the transmitter and the receiver to the performance bound of the CSI approach. Moreover, we shed light on the insight into the design of the CSI localization systems. In particular, we show that the CSI approach presents varying performance for localizing targets in different distances and directions with respect to the CSI retrieving anchor point (AP), and the geometric distribution of AP antennas could fundamentally influence the localization performance. Comprehensive experimental results are demonstrated to validate our theoretical analysis.

Index Terms—Localization, channel state information, CRB

1 Introduction

Wireless indoor localization has drawn much attention in the past decades, and enjoyed flourishing advances in recent years. Several recent work utilizes the channel state information (CSI) observed at the anchor point to estimate the location of the mobile device [15], [18], [19], [20], which achieves much higher localization accuracy level (centimeters) in contrast to that of traditional received signal strength (RSS) fingerprinting approaches (meters) [6], [7], [8], [9], [10], [11], [12], [13]. This is because CSI obtained by direct physical-layer sampling provides a finer-grained profiling of wireless signals, which can help estimate the device's possible location in a finer granularity.

However, the overwhelming majority of commodity wireless devices do not provide interfaces accessing the CSI due to the risk of technical secrets leakage. The Intel 5300 toolkit is the first tool that provides CSI interface, which is adopted by most of the work on CSI localization [15], [18], [19], [20]. The CSI is used to derive the angle-of-arrival (AoA) and time-of-flight (ToF) of the received waveform, and the amplitude information is used to crosscheck the preliminary localization result based on AoA and ToF [18]. The major challenge in such systems is the imprecise AoA and ToF measurement resulted from the multipath effect and asynchronization, for which mechanisms picking out CSI along the direct-path and eliminating clock differences are proposed. SpotFi [18] proposes a super-resolution AoA estimation scheme based on the MUSIC algorithm [27] to deal with the multipath effect, where a sanitization algorithm for estimating the measurement error is proposed; Chronos [15] utilizes inverse non-uniform discrete Fourier transformation (NDFT) to obtain the multipath profile; ToneTrack [37] utilizes the high sampling frequency of Rice WARP platform [40] to neutralize the asynchronization effect.

While CSI based localization systems can achieve admirable accuracy, the fundamental limits of CSI based localization approach itself is still unknown in a theoretical perspective. Intuitively, if precise AoA or ToF along the direct path could be obtained, there should be no error with CSI approach; however, we can still observe the localization discrepancy, because the wireless signal propagated to the receiver side has been polluted by the inevitable white noise. The root cause of localization errors with the CSI approach is actually in the nature of wireless communication. It is necessary to theoretically analyze the localization performance of the CSI based approach in the signal waveform level, only by which we can shed light on the fundamental limits the approach can achieve, and reveal the insight into the design of such systems.

The Fisher information theory has been used to analyze the information-theoretical bound of localization techniques [32], [33], [34], [35], where the basic idea is to find the Fisher information matrix (FIM) leveraging the intrinsic connection between the true value of the unknown parameter needs to be estimated and observable random variables. The inverse of the FIM is known as the Cramér-Rao bound (CRB) or Cramér-Rao lower bound (CRLB) indicating the variance of the estimated value of the unknown parameter to the true value. However, the results in the literature are either based on inaccurate radio propagation model [32], [33], [34] or impractical assumption of the received waveform [35], which are not verified by practical experiments.

- The authors are with the School of Electronic Information and Electrical Engineering, Shanghai Jiao Tong University, Shanghai 200240, China.
E-mail: {xtian, zhusujie, qq420778733, emberspirit, yangyuchengalbert, xwang8}@sjtu.edu.cn.

Manuscript received 8 Aug. 2017; revised 5 Aug. 2018; accepted 29 Aug. 2018. Date of publication 3 Sept. 2018; date of current version 28 June 2019.
(Corresponding author: Xiaohua Tian.)
For information on obtaining reprints of this article, please send e-mail to: reprints@ieee.org, and reference the Digital Object Identifier below.
Digital Object Identifier no. 10.1109/TMC.2018.2868680

In this paper, we present an information-theoretical analysis of the CSI based indoor localization approach in the received waveform level to explore fundamental limits of the approach. The theoretical findings also reveal insight into the design of CSI based localization systems. We implement essential schemes presented in recent CSI localization systems to verify our analysis. Our contributions are as following:

First, we present the CRB for the location estimation technique based on CSI. In contrast to previous work in the literature with a strong assumption of availability of the analog received waveform, our analysis is based on waveform information after the analog-to-digital converter (ADC), which is in accordance with the practical capability of the Intel 5300 toolkit. We present a frequency domain analysis to interpret how eliminating the multipath effect can influence the performance of CSI approach in a theoretical perspective (Section 4.1). Our analysis resolves the issue of high-dimensional FIM caused by utilizing antenna array in practical systems (Section 4.2); moreover, we transform the error bound for estimating the amplitude and delay of the received signals into that for localization, based on which we derive a close-form CRB for indoor localization with the CSI approach (Section 4.2). We further analyze the influence of the asychronization effect, where it is found that the noise rather than the asynchronization is the dominant factor impacting the performance of the CSI approach (Section 5).

Second, we reveal insight into the design of CSI localization based on the derived localization error bound (Section 6). We theoretically confirm the applicability of the derived CRB to all localization systems utilizing CSI observed with the Intel 5300 toolkit. We also show that: the CSI approach presents varying performance for localizing targets in different distances and directions with respect to the CSI retrieving anchor point; the geometric distribution of antennas could fundamentally influence the localization performance. In particular, the system with antennas non-uniformly spaced and the one with uniformly spaced antennas present different performance theoretically and practically.

Third, we conduct comprehensive experiments to verify our theoretical analysis (Section 7), for which we build the Wi-Fi anchor point with the mini PC and the Intel 5300 toolkit for retrieving CSI. We compare the theoretical location estimation error bound with the errors observed in practical localization process, and find that the two trends are in line with each other.

Our theoretical analysis and experiments reveal the following design guidelines for CSI localization system developers utilizing the Intel 5300 toolkit:

- The CSI localization approach can achieve millimeter-level accuracy theoretically, if the target is in opposite of the antenna array and the distance between the array and the target is around 1 meter. The distance and orientation between the antenna array and the target can influence the localization performance, which is corroborated by the experimental results. The nearer the target is to the antenna and the closer the target is to the vertical direction of the antenna array, the higher accuracy the localization approach can achieve.
- Hardware asynchronization and communication noise can impact CSI localization performance in practice, which results in practical localization errors ranging from tens to thousands of centimeters. Ideally-strict synchronization can help improve practical localization accuracy; however, in the information-theoretical perspective, the effect of noise is the dominant factor for the CSI localization system to achieve the theoretical lower performance bound.
- Due to the lack of perfect synchronization mechanism between the target and the AP in practice, the ToF can be derived from existing CSI localization mechanism [18] is unreliable; the AoA measurement can be obtained from multiple APs are the main basis for location estimation, which however are significantly impacted by the RF oscillator phase offset between antennas of the AP. The phase offset can be calibrated with the method as described in [20].
- The theoretical lower bound of the localization error with non-uniformly spaced antenna array is lower than that with uniformly spaced antenna array, and the experimental results also show that the former design yields better performance in practice. Environments also can influence the localization performance due to the multipath effects; however, the influence of distance and orientation on the localization performance is still notable.

2 Related Work

2.1 Wi-Fi Indoor Localization

Accurate indoor localization is the fundamental enabler technology of a smart world [1], where wireless techniques have been applied in the past decades. Early wireless indoor localization systems such as Active Badge [2], Bat [3] and Cricket [4] require buildings to install dedicated RF/ultrasound infrastructure. With the proliferation of Wi-Fi enabled mobile devices, the received signal strength (RSS) based indoor localization methodology is widely studied, which leverages ubiquitous Wi-Fi access points (APs) and RSS information readily available from commodity hardware. With the RSS information, the localization system utilizes radio propagation models [5] to derive the distance between the target and APs and then triangulate the location of the target, which is known as model-based approach [6], [7], [8]. The RSS information also can be used to build the radio fingerprints map, and the localization system compares the currently observed RSS information of a mobile device with the map and estimate the user's current location, which is known as fingerprinting-based approach [9], [10], [11], [12], [13]. However, the RSS methodology only achieves meter-level localization accuracy, since the RSS is a very coarse description of wireless signals. Recent work on fingerprinting localization [14] studies how to mitigate the effort of the site survey process for building the fingerprints map, which considers the shopping mall scenario. In particular, it shows that the system can direct the customer to any shop in the mall as long as the RSS values in the entrance of those shops are available.

Direct physical-layer sampling provides a finer-grained profiling of wireless signals, which offers better localization accuracy in the centimeter-level. The Intel 5300 toolkit [21] is widely used in recent years, which provides access to CSI of the wireless signal over multiple antennas. Chronos system [15] computes the ToF of the signal to derive the distance between the anchor point and the target. The SpotFi [18] localization server analyzes CSI including ToF and

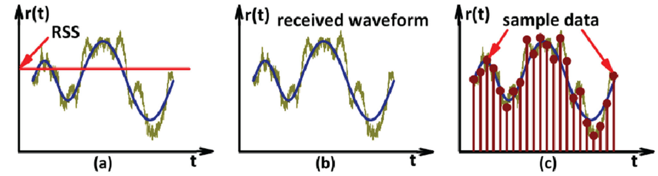

Fig. 1. The RSS and CSI of the received waveform.

AoA collected from different anchor points, and then identifies the direct path profile between the target and each AP, which are used for final location estimation. Ubicarse system [19] utilizes the principle of synthetic aperture radar (SAR) for localizing mobile devices. ArrayTrack system [20] derives the AoA information of the user's frame with respect to multiple antennas. The AoA information is then aggregated and computed to estimate the user's location. In contrast to the work mentioned above focusing on system implementation, our work in this paper studies the information-theoretical limits of the CSI approach, based on which we reveal insight into the design of the CSI based systems.

We note that Atheros [39] is another toolkit recently released for CSI retrieval, which supports a number of NICs; however, the adoption of the tool for localization is still limited according to its official webpage [41].

2.2 Cramér-Rao Bound (CRB) Analysis for Localization

Chandrasekaran et al. conducts extensive experiments to obtain an empirical quantification of the accuracy limits of RSS localization [24]; the experimental results are compared with a theoretical bound derived using CRB analysis, which is to provide a lower bound on the variance achievable by any unbiased estimator, and has been used to evaluate the performance of cooperative localization in wireless sensor networks (WSNs) [32], [33]. In the WSN case, there are normally some anchor nodes whose locations are known, and unknown-location sensors can estimate locations of themselves by conducting distance measurements between pairs of sensors. CRB analysis can help revealing the best such cooperative localization can possibly achieve. Further, classical CRB analysis can be extended to investigate the influence of misplacement of anchor nodes in wireless sensor networks [34].

However, the comparison between the theoretical bound and experimental results shows that the derived CRB for RSS based localization is inaccurate [24], [36], because RSS based approach utilizes a metric of the received waveform at the anchor point RSS for localization as shown in Fig. 1a. Most of such CRB analysis adopts the log-normal path loss (LNPL) model [24], [32], [33], [34], [36] to associate RSS with radio propagation distance, which has been proved inaccurate for indoor localization [30]. Shen et al. present the CRB analysis for localization systems utilizing the entire received waveform as shown in Fig. 1b rather than a metric of the waveform, which presents a more accurate bound [35].

The derivation of the bound in [35] relies on a strong assumption of the availability of analog waveform, which is infeasible in the CSI localization scenario since the Intel 5300 toolkit could only retrieve the sampled waveform as shown in Fig. 1c. The analysis in [35] is in the time domain, yielding very complicated theoretical results, which contain the derivative of the waveform thus can hardly reveal the insight into the system design. In order to obtain the concrete simulation results, it is assumed in [35] that the received waveform is the Gaussian pulse, which has a special property that its derivative is still in the similar form of Gaussion pulse. This is significantly helpful for simplifying the simulation process but far away from the practical situation. Moreover, the analysis in [35] just considers the single antenna anchor point, but the practical CSI localization system normally needs to utilize multiple antennas, which will make the rank of the time domain Fisher information matrix even higher. Thus it will be more difficult to obtain the concrete theoretical results that are meaningful for guiding practical system design. Our work in this paper studies the more practical bound based on the received waveform after sampling; we perform frequency domain CRB analysis to simplify the mathematical derivation, and take the practical antenna array in the anchor point into account. Our analysis can obtain close-form theoretical results that can help reveal interesting insight into the CSI approach.

Besides being applied in ordinary localization cases, CRB analysis is also utilized to medical scenario recently. Geng et al. use 3D Posterior Cramér-Rao Lower Bound (PCRLB) as a framework to evaluate accuracy of the hybrid RF and image processing localization technique for the wireless capsule endoscopy (WCE) inside the human body [31].

3 System Model

3.1 Signal Model

We consider an indoor space installed with multiple CSI retrievable anchor points. As in existing CSI based localization systems [15], [18], [19], [20], those anchor points can retrieve the CSI of wireless signals sent from the user's mobile device. Ideally, the anchor point should have perfect knowledge of the received waveform, based on which the user's location can be estimated. The received waveform can be modeled as

$$r(t) = \sum_{p=1}^{l} \alpha^{(p)} s(t - \tau^{(p)}) + z(t), \tag{1}$$

where $s(t)$ denotes the transmitting waveform, l represents the number of paths the signal experienced since transmitted, $\alpha^{(p)}$ is the amplitude of the waveform over the pth path, $\tau^{(p)}$ is the time delay of the signal over the pth path, and $z(t)$ is the additive white noise which can be regarded as a zero-mean Gaussian process with covariance σ^2. Note that $\sigma^2 = N_0/2$ and $N_0/2$ is the two-side power spectral density. The model above is a fundamental description of the received waveform in digital communication, which considers fading, multipath effect, propagation delay and noise.

However, the Intel 5300 toolkit is unable to provide CSI of the perfect analog waveform. The CSI can be used for analysis is in fact reflected by the amplitude and phase information of the waveform, which is obtained after the analog signal goes through the ADC module according to basic principles of digital communication. After the ADC module, the analog waveform is sampled and quantized. Since most of the work [15], [18], [19], [20] uses the phase information of the waveform to derive the distance between the anchor point and the mobile device, and the quantization process has small influence on the amplitude of the waveform, the waveform modeled in Eq. (1) after the sampling process becomes

$$X_m = r(mT) = \sum_{p=1}^{l} \alpha^{(p)} s(mT - \tau^{(p)}) + z(mT), \tag{2}$$

with $m = 1, \ldots, L$, where L denotes the total number of samplings and T is the sampling period. Due to the additive Gaussian white noise, the sampled value from the waveform obeys the Guassion distribution $X_m \sim N(\sum_{p=1}^{l} \alpha^{(p)} s(mT - \tau^{(p)}), \sigma^2)$, where σ^2 is the variance. After sampling, we obtain a series of Gaussian random variables and the covariance between any two variables is equal to zero with the property of Gaussian process:

$$\begin{cases} cov(X_i, X_j) = E(z(iT) \cdot z(jT)) = 0 (i \neq j); \\ cov(X_i, X_j) = D(X_i) = D(X_j) = \frac{N_0}{2} (i = j). \end{cases} \tag{3}$$

3.2 Problem Formulation

The basic idea of the CSI localization approach is to derive geometric relationship between the target and antenna array equipped on the anchor point. In particular, AoA method tries to find the propagation direction of the received waveform, and ToF method tries to find the flying time of the received waveform incident on each antenna in the antenna array. Such information is basically derived from the phase information of the waveform [15], [18], [19], [20]. Efforts also have been made to utilize the amplitude information to further improve the accuracy [18]. Consequently, the performance of CSI localization depends on how accurately the ampltitude ($\alpha^{(p)}$) and phase ($\tau^{(p)}$) information of the received waveform can be measured. Our strategy is to first find the error bound for measuring $\alpha^{(p)}$ and $\tau^{(p)}$, and then explore the corresponding error bound of location estimation.

In the location estimation process, the unknown parameter vector $\boldsymbol{\theta}$ can be formulated as

$$\boldsymbol{\theta} = [\tau^{(1)}, \alpha^{(1)}, \tau^{(2)}, \alpha^{(2)}, \ldots, \tau^{(l)}, \alpha^{(l)}]. \tag{4}$$

The basis for estimating the parameter vector is the sampled value of the received waveform, which is in fact a vector of random variables $\mathbf{X}$ as shown in Eq. (2). According to the Fisher information theory, the Fisher Information Matrix (FIM) can be calculated as

$$\mathbf{I}(\boldsymbol{\theta})_{i,j} = -\mathbf{E}\left[\frac{\partial^2}{\partial\theta_i\,\partial\theta_j} \log f(\mathbf{X}; \boldsymbol{\theta}) \middle| \boldsymbol{\theta}\right], \tag{5}$$

where $f(\mathbf{X}; \boldsymbol{\theta})$ is the probability density function (PDF) of the observed random variables, θ_i and θ_j are the unknown parameters to be estimated respectively.

Then, the parameter vector $\boldsymbol{\theta}$ satisfies the information inequality:

$$\mathbf{E}[(\hat{\boldsymbol{\theta}} - \boldsymbol{\theta})(\hat{\boldsymbol{\theta}} - \boldsymbol{\theta})^{\mathrm{T}}] \succeq \mathbf{I}^{-1}(\boldsymbol{\theta}), \tag{6}$$

where $\mathbf{A} \succeq \mathbf{B}$ means that $\mathbf{A} - \mathbf{B}$ is positive semidefinite. The inverse of the FIM can be used to evaluate the estimation accuracy of the parameter $\boldsymbol{\theta}$, in particular the variance of the estimated value of the parameter compared with the true value, which is known as the CRB.

Since the PDF $f(\mathbf{X}; \boldsymbol{\theta})$ is following Gaussian distribution according to the signal model, the FIM in this case is for an N-variate Gaussian distributed random variable $\mathbf{X} \sim \mathcal{N}(\boldsymbol{\mu}(\boldsymbol{\theta}), \Sigma(\boldsymbol{\theta}))$, where $\boldsymbol{\theta}$ is a K-dimensional vector of parameters $[\theta_1, \ldots, \theta_K]^{\mathrm{T}}$, $\mathbf{X}$ is the vector of observable random normal variables $[X_1, \ldots, X_N]^{\mathrm{T}}$ with mean $\boldsymbol{\mu}(\boldsymbol{\theta}) = [\mu_1(\boldsymbol{\theta}), \ldots, \mu_N(\boldsymbol{\theta})]^{\mathrm{T}}$ and $\Sigma(\boldsymbol{\theta})$ denotes the covariance matrix of $\mathbf{X}$. The covariance matrix is a constant diagonal matrix because any two random variables are independent to each other. Then the element in the mth row and nth column of the FIM is:

$$\mathbf{I}_{m,n} = \frac{\partial \boldsymbol{\mu}^{\mathrm{T}}}{\partial\theta_m} \Sigma^{-1} \frac{\partial \boldsymbol{\mu}}{\partial\theta_n}. \tag{7}$$

3.3 Challenges

Finding Inverse of FIM. Based on the formulation above, we need to find the expression of each element of the FIM to find the CRB; however, the inverse of the FIM with elements as mentioned above can not be found in practice, because the element of the FIM can be explicitly expressed only if the first order derivative of the received waveform can be found. This is almost impossible in practice because the Intel 5300 NIC adopts orthogonal frequency-division multiplexing (OFDM) technique, which makes the expression of the signal $s(\cdot)$ unavailable. In particular, the signal is factually an aggregation of the source signal modulated with a bunch of orthogonal sub-carriers. According to 802.11n standard [16], there are totally 56 sub-carriers at 2.4 GHz and 114 at 5 GHz; however, the CSI can be observed is only for 30 sub-carriers [17], [18]. This means that although we could know which 30 sub-carriers are used based on 802.11n standard [16] , the general form of $s(\cdot)$ is unknown for all the sub-carriers. Moreover, the expression of $s(\cdot)$ also depends on the source code, which is also unavailable from Intel 5300 toolkit. Consequently, although the expression of the inverse of the FIM and the CRB can be given in certain form, the results make nonsense in terms of revealing the insight of CSI approach or guiding the design of CSI based localization system.

Multipath Effect. The fundamentals of the Fisher information theory are that the unknown parameters and the observable random variables are intrinsically connected; however, it is usually difficult to find such intrinsic connection. The radio propagation model such as LNPL indicates the connection between the RSS and distance, but the empirical association hardly reflects the real situation, as the multipath effect is not fully considered in the model. This is why the CRB based on such connection has been proved inaccurate for the RSS based localization [24]. The multipath effect also impacts the performance of the CSI based approach [15], [18], [20]. In particular, CSI approach is interested in only the amplitude and phase information of the received waveform along the direct path, which can be denoted using $\alpha^{(1)}$ and phase $\tau^{(1)}$, respectively. However, we are unable to just regard $\alpha^{(1)}$ and $\tau^{(1)}$ as the parameter, since in this way the connection between these parameters and the signal model is unable to reflect the real situation, which results in incorrect CRB.

Asynchronization. Asynchronization between the transmitter and the receiver is incurred by crystal oscillating circuits implementations, which is inevitable even for devices by the same manufacturer. The asynchronization leads to a sampling frequency offset, which further causes a time shift impacting the phase measurement. Recent work [18], [19], [20], [37], [39] propose methods to remove the asynchronization effect; however, the key issue that whether the asynchronization effect is the dominant factor of localization errors is still unknown.

Antenna Array and Design Guidance. The problem formulation with Fisher information theory just considers the received waveform from one antenna; however, the practical CSI approach normally utilizes the antenna array. More antennas will incur the high-rank FIM, which imposes challenges to find the inverse of the FIM. Since antennas are independent with each other in localization, how to aggregate contributions of all antennas to evaluate the overall performance of the localization system is challenging. Moreover, after obtaining the CRB bound, we must reveal the insight into the CSI localization system design, in order to guide improving the system performance.

Our solutions to deal with the challenges mentioned above will be presented in the following sections.

4 CRB Analysis in Frequency Domain

This section deals with the first two challenges. In order to perform localization, we are actually interested in parameter $\boldsymbol{\theta}_1 = [\tau^{(1)}, \alpha^{(1)}]$, which are the received signal's properties along the direct path from the transmitter to the receiver. This requires revealing the multipath profile so that the direct path component can be picked out. To this end, the Chronos system [15] utilizes the inverse DFT to analyze the multipath effect to obtain the multipath profile. The smart idea of the Chronos system inspires us to perform the CRB analysis in the frequency domain, which makes it possible to find the inverse of FIM.

In the following, we first examine an ideal case that the parameter can be measured with single antenna, and then extend our analysis to the practical scenario involving the antennas array.

4.1 Parameter Analysis with Single Antenna

Consider the signal along the direct path in the time domain

$$r(nT) = \alpha^{(1)} s(nT - \tau^{(1)}) + z(nT), \tag{8}$$

where $n = 1, 2, 3, \ldots, L$. We can apply L-point DFT to the waveform to get the counterpart expression in the frequency domain

$$R(k) = \alpha^{(1)} S(k) e^{-j\frac{2\pi k \tau^{(1)}}{LT}} + \eta(k), \tag{9}$$

with $k = 0, 1, 2, \ldots, L-1$, where the signal spectrum $S(k)$ depends on the transmitting waveform that is usually fixed, $\eta(k)$ is the power spectrum of white Gaussian noise with covariance $L\sigma^2$.

Leveraging the multipath profiling technique mentioned in [15], the previous parameter vector can be cut down to $\boldsymbol{\theta}_1$, and we can establish an accurate intrinsic connection between unknown parameters $\boldsymbol{\theta}_1$ and the observable random variables $S(k)$. We use τ and α to replace $\tau^{(1)}$ and $\alpha^{(1)}$ in rest of the section for simplicity. The observations incorporate all samples of the received signal in the frequency domain. We use vector $\mathbf{X}$ to denote all the random variables:

$$\mathbf{X} = [R(0), R(1), \ldots, R_1(L-1)]^{\mathrm{T}}, \tag{10}$$

where the mean vector $\boldsymbol{\mu}$ for the variable vector $\mathbf{X}$ is:

$$\boldsymbol{\mu} = \left[\alpha S(0) e^{-j\frac{2\pi 0 \tau}{LT}}, \ldots, \alpha S(L-1) e^{-j\frac{2\pi (L-1)\tau}{LT}}\right]^{\mathrm{T}}. \tag{11}$$

With the complex mean vector in the frequency domain, the element of the FIM extended for complex data can be derived [29]

$$\mathbf{I}_{mn} = 2Re\left[\frac{\partial \boldsymbol{\mu}^{\mathrm{H}}}{\partial \theta_m} \sum\nolimits^{-1} \frac{\partial \boldsymbol{\mu}}{\partial \theta_n}\right], \tag{12}$$

where $\sum$ is the covariance matrix which is equal to $L\sigma^2$ and H denotes the complex conjugate transpose of the matrix. The FIM for single antenna in frequency domian is

$$\mathbf{I} = \frac{2}{L\sigma^2} \begin{bmatrix} \sum_{k=0}^{L-1} 4\pi^2 \left(\frac{k}{LT}\right)^2 \alpha^2 |S(k)|^2 & 0 \\ 0 & \sum_{k=0}^{L-1} |S(k)|^2 \end{bmatrix}. \tag{13}$$

We here provide the CRB for estimating the delay τ, which is the parameter of interest in both ToF and AoA. The squared error bound with respect to τ is

$$\mathbf{E}\{(\hat{\tau} - \tau)^2\} = \mathbf{Var}(\tau) \geq [\mathbf{I}(\theta)^{-1}]_{1\times 1}, \tag{14}$$

where $[\cdot]_{n\times n}$ denotes the upper left $n \times n$ submatrix of the arguments.

Consequently, the CRB for the time delay with CSI approach termed as time delay error bound (TDEB) in the frequency domain utilizing the FIM in Eq. (13) is

$$\mathcal{T}(\tau) = \frac{L^3 T^2 \sigma^2}{8\pi^2 \alpha^2} \frac{1}{\sum_{k=0}^{L-1} k^2 |S(k)|^2}. \tag{15}$$

We can further simplify the bound with the corresponding channel impulse response (CIR), where $s(t)$ is $\delta(t)$ and $|S(k)| = 1$ for $k = 0, 1, \ldots, L-1$. Thus the bound becomes

$$\mathcal{T}(\tau) = \frac{3L^2 T^2 \sigma^2}{4\pi^2 \alpha^2 (L-1)(2L-1)}. \tag{16}$$

4.2 Parameter Estimation with Antenna Array

The analysis above shows the feasibility of performing CRB in the frequency domain with the idea single antenna case; however, the practical mechanism that can obtain the ToF with the single antenna is still unavailable to the best of our knowledge. All existing work in the literature requires using information from multiple antennas at the receiver side, especially the system depending on AoA information to perform location estimation. Consequently, we now try to find the parameter estimation error bound with antennas array.

Suppose there are N antennas at the receiver side, then the received signal of the mth antenna along the direct path at sampling time point n in the time domain can be expressed as:

$$r_m(nT) = \alpha_m s(nT - \tau_m) + z(nT), \tag{17}$$

with $m = 1, 2, 3, \ldots, N$, $n = 1, 2, 3, \ldots, L$.

The parameter α_m and τ_m denote the amplitude and the time delay of the received waveform along the direct path incident to the mth antenna, and $z(nT)$ denotes the noise effect which is normally following Gaussian distribution, with sampling period T and the total number of samples L. It is reasonable to assume that the total number of samplings for each antenna in the array is the same, since those antennas in the array normally share an ADC module at the receiver in practice. The signal as shown in (17) can be transformed into the frequency domain with L-point DFT, which becomes

$$R_m(k) = \alpha_m S(k) e^{-j\frac{2\pi k \tau_m}{LT}} + \eta(k), \tag{18}$$

where $k = 0, 1, 2, \ldots, L-1$ and $m = 1, 2, 3, \ldots, N$. The parameter $\eta(k)$ is the zero-mean complex white Gaussian noise with the covariance $L\sigma^2$. The signal power spectrum

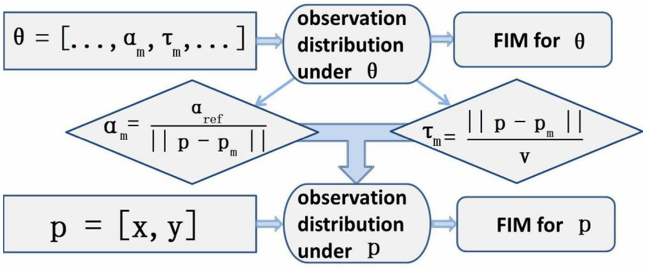

Fig. 2. Strategy of CRB for location estimation with antenna array.

$S(k)$ depends on the transmitting waveform; therefore, it is reasonable to assume that the signal spectrum $S(k)$ is the same for the receiver waveforms over all antennas.

Since there are N antennas at the receiver, the parameter vector to be estimated is

$$\boldsymbol{\theta} = \underbrace{[\tau_1, \alpha_1, \tau_2, \alpha_2, \ldots, \tau_N, \alpha_N]}_{2N}. \tag{19}$$

The observable random variables are the collection of all the received waveform in the frequency domain over the sampling time. We use vector $\mathbf{X}$ to denote the $NL \times 1$ dimensional random variables:

$$\begin{aligned}\mathbf{X} = \ & \underbrace{[R_1(0), R_1(1), \ldots, R_1(L-1)}_{antenna1}, \ldots\ldots \\ & \underbrace{R_N(0), R_N(1), \ldots, R_N(L-1)}_{antennaN}]^{\mathrm{T}}.\end{aligned} \tag{20}$$

Since the parameter $\eta(k)$ is the zero-mean complex white Gaussian noise, the mean vector $\boldsymbol{\mu}$ of $\mathbf{X}$ is:

$$\begin{aligned}\boldsymbol{\mu} = \ & \underbrace{[\alpha_1 S(0), \alpha_1 S(1) e^{-j\frac{2\pi\tau_1}{LT}}, \ldots, \alpha_1 S(L) e^{-j\frac{2\pi(L-1)\tau_1}{LT}}}_{antenna_1}, \ldots\ldots \\ & \underbrace{\alpha_N S(0), \alpha_N S(1) e^{-j\frac{2\pi\tau_N}{LT}}, \ldots, \alpha_N S(L) e^{-j\frac{2\pi(L-1)\tau_N}{LT}}}_{antenna_N}]^{\mathrm{T}}.\end{aligned} \tag{21}$$

With the analysis above, it seems that we could find the inverse of the FIM and then derive the CRB the same way as for the single antenna case like Eq. (12); however, it can be found that the introduction of multiple antennas makes the rank of the corresponding FIM high along this vein. In particular, it is well known that the Intel 5300 NIC has three slots for antennas, which makes the rank of the FIM to be 6 (with the amplitude and the delay). The receiver in the Arraytrack [20] system has 8 antennas, which makes the rank to be 16. It is tractable to numerically find the inverse of the 6/16-rank FIM; however, it is unlikely to present the corresponding close-form CRB, without which it is impossible to reveal any insight into the CSI approach.

Moreover, even if we could obtain close-form CRB with the high-dimensional FIM, the information-theoretical bound is for estimating the parameters αs and τs, but our ultimate goal is to find the bound for estimating location of the target. Each single antenna plays the unique role in the localization process, and how to incorporate contributions of all antennas in the array to derive the CRB is still unknown in the literature to the best of our knowledge.

4.3 CRB for Location Estimation

Our strategy to deal with the two issues mentioned above is to associate the parameters αs and τs with location estimation, which is shown in Fig. 2. We could observe sampled waveform as a set of random variables $\mathbf{X}$ which represent the effect of parameters τs and αs. We use $\mathbf{p}$ to denote the position of the target, and $\mathbf{p_m}$ the position of the mth antenna in the 2-D euclidean space. It is straightforward that

$$\tau_m = \frac{||\mathbf{p} - \mathbf{p}_m||}{v}, \tag{22}$$

where v is the speed of light.

With the multipath profiling technique in [15], we could pick out the CSI over the direct path. Since the influence of small scale fading caused by multipath effect can be ignored, the amplitude of the received waveform is only related to the distance between the transmitter and the receiver. In most of the localization systems with CSI approach, the transmitter of the target is basically equipped with the omnidirectional antenna [15], [18], [19], [20], which means that the transmitted waveform can be modeled as a spherical wave, and the amplitude of the wave decreases with the distance of propagation. Note that the power of the transmitted waveform is inversely proportional to the square of the propagation distance, but our analysis is in the received waveform level. Thus we have

$$\alpha_m = \frac{\alpha_{ref}}{||\mathbf{p} - \mathbf{p}_m||}, \tag{23}$$

where α_{ref} is the reference amplitude at $1m$ away from the transimitter.

We now could obtain a new parameter for estimation based on the analysis above. Since CSI based approaches need to utilize the geometric relationship between the transmitter and the anchor points, the precise location information of the anchor points and antenna on them is usually perfectly known. We use $\mathbf{p_1}, \mathbf{p_2}, \ldots, \mathbf{p_N}$ to denote locations of antennas, based on which we can construct a new parameter vector for estimation $\boldsymbol{\theta} = [\mathbf{p}^{\mathrm{T}}] = [x, y]$, as shown in Fig. 2.

With such a parameter transformation, we could use Fisher information theory to find the CRB for location estimation with CSI approach as shown in Fig. 2. The rank of the parameter to be estimated is reduced from $2N$ to 2, and

$$\mathbf{H}^H = \begin{bmatrix} \alpha_{\mathrm{ref}} S^*(0) e^{j\frac{2\pi\cdot 0||\mathbf{p}-\mathbf{p}_m||}{LTv}} \left(-\frac{1}{||\mathbf{p}-\mathbf{p_1}||^2} + j\frac{2\pi\cdot 0}{LTv||\mathbf{p}-\mathbf{p_1}||}\right) \frac{\mathbf{p}^{\mathrm{T}}-\mathbf{p}_1^{\mathrm{T}}}{||\mathbf{p}-\mathbf{p_1}||} \\ \vdots \\ \alpha_{\mathrm{ref}} S^*(k) e^{j\frac{2\pi k||\mathbf{p}-\mathbf{p}_m||}{LTv}} \left(-\frac{1}{||\mathbf{p}-\mathbf{p}_m||^2} + j\frac{2\pi k}{LTv||\mathbf{p}-\mathbf{p}_m||}\right) \frac{\mathbf{p}^{\mathrm{T}}-\mathbf{p}_m^{\mathrm{T}}}{||\mathbf{p}-\mathbf{p}_m||} \\ \vdots \\ \alpha_{\mathrm{ref}} S^*(L-1) e^{j\frac{2\pi(L-1)||\mathbf{p}-\mathbf{p}_m||}{LTv}} \left(-\frac{1}{||\mathbf{p}-\mathbf{p}_N||^2} + j\frac{2\pi(L-1)}{LTv||\mathbf{p}-\mathbf{p}_N||}\right) \frac{\mathbf{p}^{\mathrm{T}}-\mathbf{p}_N^{\mathrm{T}}}{||\mathbf{p}-\mathbf{p}_N||} \end{bmatrix}^T_{LN\times 1} \tag{24}$$

$$tr\{\mathbf{I}^{-1}\} = \frac{L\sigma^2}{2\alpha_{ref}^2} \frac{\sum_{m=1}^{N} \frac{1}{\beta_m^2}}{\left(\sum_{m=1}^{N} \frac{1}{\beta_m^2} \cos^2(\theta_m)\right)\left(\sum_{m=1}^{N} \frac{1}{\beta_m^2} \sin^2(\theta_m)\right) - \left(\sum_{m=1}^{N} \frac{1}{\beta_m^2} \cos(\theta_m)\sin(\theta_m)\right)^2} \tag{29}$$

the rank of the FIM is reduced to 2; moreover, we could find the estimation error for localization.

In particular, we first find the FIM $\mathbf{I} = 2Re[\mathbf{H}^H \sum^{-1} \mathbf{H}]$, where $\mathbf{H}$ can be obtained by finding the first derivative of Eq. (21) with respect to $\mathbf{p}^{\mathrm{T}}$ and H denotes the complex conjugate transpose. The the result of $\mathbf{H}^H$ is shown in Eq. (24). Consequently, the corresponding FIM is

$$\mathbf{I} = \frac{2\alpha_{ref}^2}{L\sigma^2} \sum_{m=1}^{N} \sum_{k=0}^{L-1} |S(k)|^2 \left(\frac{1}{\rho_m^4} + \frac{4\pi^2 k^2}{L^2 v^2 T^2 \rho_m^2} \right) \mathbf{D}_m, \tag{25}$$

where $\mathbf{D}_m$ is a function of $\frac{\mathbf{P}-\mathbf{P}_m}{\|\mathbf{P}-\mathbf{P}_m\|}$. The expression of $\mathbf{D}_m$ is too complicated for us to find the close-form inverse of $\mathbf{I}$, thus we switch to polar coordinates system, where the origin of the system is set at the target's location. Then we can find

$$\mathbf{D}_m = \begin{bmatrix} \cos^2(\theta_m) & \cos(\theta_m)\sin(\theta_m) \\ \cos(\theta_m)\sin(\theta_m) & \sin^2(\theta_m) \end{bmatrix},$$

with θ_m denotes the angle to the mth antenna with respect to the origin.

We let

$$\frac{1}{\beta_m^2} = \sum_{k=0}^{L-1} |S(k)|^2 \left(\frac{1}{\rho_m^4} + \frac{4\pi^2 k^2}{L^2 v^2 T^2 \rho_m^2} \right), \tag{26}$$

for convenience of demonstration, and then we have

$$E\{(\hat{\mathbf{p}} - \mathbf{p})(\hat{\mathbf{p}} - \mathbf{p})^{\mathrm{T}}\} \succeq \mathbf{I}^{-1}, \tag{27}$$

according to the Fisher information theory, based on which we can find the variance of the CSI localization with antenna array:

$$E\{||\hat{\mathbf{p}} - \mathbf{p}||^2\} \geq tr\{\mathbf{I}^{-1}\}, \tag{28}$$

where $tr\{\mathbf{I}^{-1}\}$ is the trace of the inverse of FIM as shown in Eq. (29).

5 Asynchronization Analysis

This section resolves the third challenge mentioned in Section 3.3. We study another cause of localization error with CSI approach, clock asynchronization between the transmitter and the receiver [38]. The asynchronization is incurred by the crystal oscillating circuits in different hardware, which is inevitable even for devices by the same manufacturer. In particular, the analog received signal goes through the ADC module at the receiver, where the analog waveform is sampled and quantized for the estimation of the CSI. The ansychronization between the transmitter and the receiver incurs a sampling frequency offset, which further causes a time shift impacting the phase measurement [39].

The time shift by clock ansychronization is unpredictable, but can be regarded as a constant during a short-time measurement as in the localization scenario; thus the time shift is a constant for different subcarriers and antennas. Let τ_0 denote the extra time shift caused by the asynchronization and $r(nT)$ from Eq. (8) denote the ideal sampling result of the received signal. The received signal under the influence of asynchronization can be modeled as:

$$\widetilde{r}(nT) = r(nT - \tau_0) = \alpha s(nT - \tau - \tau_0) + z(nT - \tau_0), \tag{30}$$

where T is the sampling period.

5.1 Parameter Estimation over Single Antenna

In this case, the received signal model in the frequency domain is the L-point DFT of the Eq. (29):

$$\widetilde{R}(k) = \alpha S(k) e^{-j\frac{2\pi k(\tau+\tau_0)}{LT}} + \eta(k) e^{-j\frac{2\pi k \tau_0}{LT}}, \tag{31}$$

where $k = 0, 1, 2, \ldots, L-1$ for L-length sampling, τ is the propagation time in the air and τ_0 is the fixed time shift due to the asynchronization.

It can be seen that the distribution of $\widetilde{R}(k)$ is now dependent on three unknowns τ, α and τ_0, thus estimation vector $\boldsymbol{\theta}$ becomes $[\tau, \alpha, \tau_0]$. Due to the property of DFT, the mean value of the received signal only contains the signal part, and the mean of $\eta(k)$ is zero. Consequently, the resulted FIM $\mathbf{I}$ of the new parameter vector $\boldsymbol{\theta}$ is:

$$\frac{8\pi^2\alpha^2}{L^3T^2\sigma^2} \begin{bmatrix} \sum_{k=0}^{L-1} k^2|S(k)|^2 & 0 & \sum_{k=0}^{L-1} k^2|S(k)|^2 \\ 0 & \frac{L^2T^2}{4\pi^2\alpha^2} \sum_{k=0}^{L-1} |S(k)|^2 & 0 \\ \sum_{k=0}^{L-1} k^2|S(k)|^2 & 0 & \sum_{k=0}^{L-1} k^2|S(k)|^2 \end{bmatrix}. \tag{32}$$

Note that FIM $\mathbf{I}$ is not full rank, since the first row and the third row are the same, which means that we are unable to find inverse of $\mathbf{I}$ thus the error of τ can not be bounded. Based on Eq. (31), the phase component of the observable random variables $R(k)$ is determined by time delay τ and time shift τ_0. For the same phase of received signal, there are innumerable solutions for τ as long as the τ_0 changes correspondingly so that $\tau + \tau_0$ remains the same, which is the fundamental reason why the inverse of FIM does not exist. The physical meaning of the result is that we are unable to estimate the parameter τ based on the observable random variables over the single antenna, because the effect of τ and τ_0 are aggregated. Without the prior knowledge of τ_0, the propagation delay measurements by the single antenna observable results are unreliability.

5.2 Parameter Estimation over Multiple Antennas

Similarly, since different antennas of the receiver share the same ADC module, the received signal model for antenna array has the same asynchronization time shift τ_0. The received signal model considering asynchronization in the frequency domain can be denoted by:

$$\widetilde{R}_m(k) = \alpha_m S(k) e^{-j\frac{2\pi k(\tau_m+\tau_0)}{LT}} + \eta(k) e^{-j\frac{2\pi k \tau_0}{LT}}, \tag{33}$$

where $k = 0, 1, \ldots, L-1$ for L-length sampling, $m = 1, 2, \ldots, N$ for N antennas, τ_m denotes the propagation time delay between the receiver's mth antenna and the transmitter.

Similar to the situation in Section 4.3, now the vector to be estimated $\boldsymbol{\theta}$ becomes:

$$\boldsymbol{\theta} = [x, y, \tau_0], \tag{34}$$

where x, y are the target's horizontal and vertical localization coordinates. The phase shift of the Gaussian noise component $\eta(k)$ has no influence on the mean vector $\boldsymbol{\mu}$ since the DFT of the Gaussian noise is still a Gaussian noise. Thus compared with Eq. (21), the mean vector $\boldsymbol{\mu}$ remains except for a phase shift in the frequency domain due to τ_0 in the time domain. To derive the FIM, we need to take the derivative of the mean vector with respect to the parameter vector. For the convenience of derivation, we use the polar coordinates to express the derivative result. The result of the FIM consists of the sum of the sampling length L and the sum of different antennas. These sums are functioned as a coefficient in the FIM. For simplification, we use the parameter β_m from Eq. (26) and let

$$\frac{1}{\gamma_m} = \sum_{k=0}^{L-1} |S(k)|^2 \frac{4\pi^2 k^2}{L^2 T^2 \rho_m^2}, \tag{35}$$

where the polar coordinate ρ_m denotes the distance between the mth antenna and the target device. Then the simplified FIM $\mathbf{I}$ of the parameter vector $\boldsymbol{\theta}$ is

$$\frac{2\alpha_{ref}^2}{L\sigma^2} \begin{bmatrix} \sum_{m=1}^{N} \frac{\cos^2\theta_m}{\beta_m^2} & \sum_{m=1}^{N} \frac{\cos\theta_m \sin\theta_m}{\beta_m^2} & \sum_{m=1}^{N} \frac{\cos\theta_m}{\upsilon\gamma_m} \\ \sum_{m=1}^{N} \frac{\cos\theta_m \sin\theta_m}{\beta_m^2} & \sum_{m=1}^{N} \frac{\sin^2\theta_m}{\beta_m^2} & \sum_{m=1}^{N} \frac{\sin\theta_m}{\upsilon\gamma_m} \\ \sum_{m=1}^{N} \frac{\cos\theta_m}{\upsilon\gamma_m} & \sum_{m=1}^{N} \frac{\sin\theta_m}{\upsilon\gamma_m} & \sum_{m=1}^{N} \frac{1}{\gamma_m} \end{bmatrix}. \tag{36}$$

We then need to find the estimation error bound of the parameter by finding the inverse of the FIM above. However, we are only interested in the first two parameters' estimation error bound, which is to be obtained with the equivalent Fisher information matrix (EFIM) for the convenience of demonstration [35].

The N-length parameter vector $\boldsymbol{\theta}$ can be divided into two parts $\boldsymbol{\theta} = [\boldsymbol{\theta}_1^T, \boldsymbol{\theta}_2^T]^T$ where n-length parameters $\boldsymbol{\theta}_1$ is of the interest. The $N \times N$ FIM $\mathbf{I}_{\boldsymbol{\theta}}$ can be divided corresponding to the parameter vector $\boldsymbol{\theta}$.

$$\mathbf{I}_{\boldsymbol{\theta}} = \begin{bmatrix} \mathbf{A} & \mathbf{B} \\ \mathbf{B}^T & \mathbf{C} \end{bmatrix}, \tag{37}$$

where $\mathbf{A} \in R^{n\times n}, \mathbf{B} \in R^{n\times(N-n)}, \mathbf{C} \in R^{(N-n)\times(N-n)}$. The submatrix $\mathbf{A}$ is corresponding to the n interested parameters in the parameter vector $\boldsymbol{\theta}$. Then the EFIM is

$$\mathbf{I}_e \triangleq \mathbf{A} - \mathbf{B}\mathbf{C}^{-1}\mathbf{B}^T, \tag{38}$$

which has the property that $[\mathbf{I}_{\boldsymbol{\theta}}{}^{-1}]_{n\times n} = \mathbf{I}_e{}^{-1}$. In particular, we are interested in the parameter $\mathbf{p}$; $\mathbf{A}$ is the upper-left 2×2 submatrix in $\mathbf{I}$ that is corresponding to the first two parameters x and y. We can derive the 2×2 EFIM from Eqs. (36) and (38). With the EFIM, according to the information inequality, we can get the variance of the CSI localization by calculating the trace of the inverse EFIM.

$$E\{||\hat{\mathbf{p}} - \mathbf{p}||^2\} \geq tr\{\mathbf{I_e}^{-1}\}, \tag{39}$$

where $tr\{\mathbf{I_e}^{-1}\}$ is shown in Eq. (40) and $tr\{\mathbf{I_e}^{-1}\}$ is the lower bound of the localization estimation error.

Observing Eq. (40), it is interesting to find that the expression of the bound is independent of τ_0, but proportional to the variance of the noise σ^2. This does not mean that the location estimation error bound is independent of the degree of asynchronization, because if this is the case, then the bounds in Eqs. (29) and (40) are supposed to be the same (Recall that Eq. (29) presents the location estimation error bound without taking asynchronization into account). This result indicates that the asynchronization effect is less effective than the wireless communication noise in impacting the fundamental performance bound of CSI localization.

Since the noise factor is dominating in determining the fundamental CSI localization performance, and the CRB considering asynchronization is over complicated, it is more reasonable to reveal the insight into the design of CSI localization systems based on the CRB shown in Eq. (29). We could try to eliminate the time shift by asynchronization as shown in [18], [19], [20], [37], [39]; however, the impact of noise is unable to be eliminated, which is the major factor incurring localization errors in CSI approach.

It is worth mentioning that the introduction of asychronization does not change the unbiasedness of the estimator. Recall that the estimator function in the synchronized case is $\hat{\mathbf{p}}(\mathbf{X})$, with $\mathbf{E}[\hat{\mathbf{p}}(\mathbf{X})] = \int \hat{\mathbf{p}}(\mathbf{X})d\mathbf{X} = \mathbf{p}$. If we take the asynchronization effect τ_0 into account, the estimator function becomes $\mathbf{E}[\hat{\mathbf{p}}(\tilde{\mathbf{X}})] = \int \hat{\mathbf{p}}(\tilde{\mathbf{X}})d\tilde{\mathbf{X}} = \int \bigcup_{m=1}^{N} \bigcup_{k=0}^{L-1} e^{-j\frac{2\pi k\tau_0}{LT}} \hat{\mathbf{p}}(\mathbf{X})d\mathbf{X} = \int (\bigcup_{m=1}^{N} 1)\hat{\mathbf{p}}(\mathbf{X})d\mathbf{X} = \mathbf{p}$, which is also a unbiased estimator. Although the asynchronization factor τ_0 does not present in Eq. (40), it changes the localization estimation error bound $tr\{\mathbf{I_e}^{-1}\}$ compared with Eq. (29). This means that the existence of time shift τ_0 actually impacts the lower error bound.

6 INSIGHT INTO CSI APPROACH

This section reveals insight into the CSI approach based on our theoretical analysis. We first simplify the form of the derived CRB. In practice, the wavelength λ of the Wi-Fi signal is around $9 - 12$ cm, much less than the distance between the target and the antenna array. Given that $\frac{4\pi^2 k^2}{L^2 \upsilon^2 T^2 \rho_m^2} \geq (\frac{2\pi}{\lambda\rho_m})^2 \gg \frac{1}{\rho_m^4}$, Eq. (26) can be simplified as $\frac{1}{\beta_m^2} \approx \sum_{k=0}^{L-1} |S(k)|^2 \frac{4\pi^2 k^2}{L^2 \upsilon^2 T^2 \rho_m^2}$.

We let $\mathcal{K} = L\sigma^2 \Big/ (2\alpha_{ref}^2 \sum_{k=0}^{L-1} \frac{4\pi^2 k^2}{L^2 \upsilon^2 T^2})$ to denote the rest part of the CRB. The denominator of Eq. (29) can be further simplified using the principles of trigonometric function, which yields

$$tr\{\mathbf{I_e}^{-1}\} = \frac{L\sigma^2}{2\alpha_{ref}^2} \frac{\sum_{m=1}^{N} \frac{1}{\beta_m^2} - \frac{\left(\sum_{m=1}^{N} \frac{\cos\theta_m}{\gamma_m}\right)^2 + \left(\sum_{m=1}^{N} \frac{\sin\theta_m}{\gamma_m}\right)^2}{\upsilon^2 \sum_{m=1}^{N} \frac{1}{\gamma_m}}}{\left(\sum_{m=1}^{N} \frac{\cos^2\theta_m}{\beta_m^2} - \frac{\left(\sum_{m=1}^{N} \frac{\cos\theta_m}{\gamma_m}\right)^2}{\upsilon^2 \sum_{m=1}^{N} \frac{1}{\gamma_m}}\right)\left(\sum_{m=1}^{N} \frac{\sin^2\theta_m}{\beta_m^2} - \frac{\left(\sum_{m=1}^{N} \frac{\sin\theta_m}{\gamma_m}\right)^2}{\upsilon^2 \sum_{m=1}^{N} \frac{1}{\gamma_m}}\right) - \left(\sum_{m=1}^{N} \frac{\cos\theta_m \sin\theta_m}{\beta_m^2} - \frac{\left(\sum_{m=1}^{N} \frac{\cos\theta_m}{\gamma_m}\right)\left(\sum_{m=1}^{N} \frac{\sin\theta_m}{\gamma_m}\right)}{\upsilon^2 \sum_{m=1}^{N} \frac{1}{\gamma_m}}\right)^2} \tag{40}$$

$$G(\mathcal{N}) = \frac{\sum_{m=1}^{N} \frac{1}{\rho_m^2}}{\sum_{m=1}^{N} \sum_{n=1}^{N} \frac{1}{\rho_m^2} \frac{1}{\rho_n^2} \sin^2(\theta_m - \theta_n)}, \tag{41}$$

where $\mathcal{N}$ denotes a set of the antennas. Thus the CRB for localization can be rewritten as

$$\mathcal{F}(\mathcal{N}) = tr\{\mathbf{I}^{-1}\} = \mathcal{K}G(\mathcal{N}), \tag{42}$$

Theorem 1. *The CRB as shown in Eq. (29) must be applicable to CSI localization approaches with Intel 5300 toolkit.*

Proof. With the analysis process presented in previous sections, we can see that the CRB can be derived as long as the inverse of the FIM can be found, which is closely related to how the hardware is processing the received waveform. We need to reveal the implicit necessary condition of finding the inverse of FIM in the analysis of previous sections, and see whether the Intel 5300 toolkit can satisfy the condition.

Consider a general case where we have an m_1-dimensional observable random variable vector with mean values $\vec{\mu} = [\mu_1, \mu_2, \ldots, \mu_{m_1}]$ to estimate m_2 parameters. Then the corresponding FIM can be denoted as $\mathbf{I} = \mathbf{U}^T\mathbf{U}$ and

$$U = \begin{bmatrix} \frac{\partial\mu_1}{\partial\theta_1} & \frac{\partial\mu_2}{\partial\theta_1} & \cdots & \frac{\partial\mu_{m_1}}{\partial\theta_1} \\ \frac{\partial\mu_1}{\partial\theta_2} & \frac{\partial\mu_2}{\partial\theta_2} & \cdots & \frac{\partial\mu_{m_1}}{\partial\theta_2} \\ \vdots & \vdots & \ddots & \vdots \\ \frac{\partial\mu_1}{\partial\theta_{m_2}} & \frac{\partial\mu_2}{\partial\theta_{m_2}} & \cdots & \frac{\partial\mu_{m_1}}{\partial\theta_{m_2}} \end{bmatrix}_{m_1 \times m_2}. \tag{43}$$

Suppose $\mathbf{U}$ is a full row or column rank matrix and $\mathbf{x}$ is the nullspace in $\mathbf{U}$, then we have $\mathbf{Ux} = \mathbf{0}$, and

$$\mathbf{Ix} = \mathbf{U}^{\mathrm{T}}\mathbf{Ux} = \mathbf{0},$$

which means that $\mathbf{x}$ is also the nullspace in $\mathbf{U}^{\mathrm{T}}\mathbf{U}$. Similarly, if $\mathbf{x}$ is the nullspace in $\mathbf{I}$, then we have

$$(\mathbf{x}^{\mathrm{T}})\mathbf{U}^{\mathrm{T}}\mathbf{Ux} = (\mathbf{Ux})^{\mathrm{T}}\mathbf{Ux} = ||\mathbf{Ux}||^2 = 0.$$

We thus have $\mathbf{Ux} = \mathbf{0}$. The homogeneous linear equation $\mathbf{Ix} = \mathbf{U}^{\mathrm{T}}\mathbf{Ux} = \mathbf{0}$ has the same basic system of solutions as $\mathbf{Ux} = \mathbf{0}$, which means that $rank(\mathbf{I}) = rank(\mathbf{U}^{\mathrm{T}}\mathbf{U}) = rank(\mathbf{U}) = min\{m_1, m_2\}$. Since $\mathbf{I}$ is an $m_2 \times m_2$ matrix, which must be full rank to find the inverse; therefore, it must be $m_1 > m_2$ so that the inverse of $\mathbf{I}$ can be found.

This means that the sufficient condition to find the inverse of the FIM is that the number of observable random variables must be greater than the number of parameters to be estimated. In our analysis in previous sections, the number of observable random variables is related to the sampling frequency, and the number of parameters to be estimated depends on how the model is constructed, which in the worst case is related to the number of paths the signal components experienced. Intel 5300 NIC's working bandwidth is 20 MHz or 40 MHz, which means that the number of observable random variables is definitely larger than the possible number of parameters to be estimated according to the Nyquist sampling theorem. That is, Intel 5300 toolkit must enable finding the inverse of the FIM, and once the inverse of the FIM can be found, we can derive the CRB as shown in previous sections. □

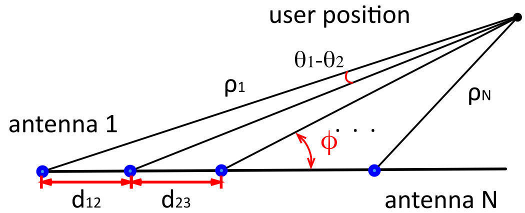

Fig. 3. Antenna array in far field.

Theorem 2. *With the CSI approach using Intel 5300 toolkit, the non-uniformly spaced antenna array outperforms the uniformly spaced one in terms of localizing the target that is far-way from the array with $\rho \gg d_{13}$, where d_{13} is the fixed distance between the 1st and the 3rd antenna in the array.*

Proof. We first consider a general case with N-antenna array; the target is faraway from the array with $\rho \gg d_{1N}$. In this case, the distance between the user and each single antenna is almost the same with $|\rho_m - \rho_n| \approx d_{mn}\cos\varphi$ as shown in Fig. 3. The parameter d_{mn} represents the distance between $antenna_m$ and $antenna_n$ and φ denotes the angle between the user position and antenna array. □

Then we have

$$\begin{aligned} \sin^2(\theta_m - \theta_n) &= 1 - \left(\frac{\rho_m^2 + \rho_n^2 - d_{mn}^2}{2\rho_m\rho_n}\right)^2 \\ &\approx 1 - \left(\frac{\rho_m^2 + \rho_n^2}{2\rho_m\rho_n}\right)^2 \left(1 - \frac{2d_{mn}^2}{\rho_m^2 + \rho_n^2}\right) \\ &= \frac{2d_{mn}^2}{\rho_m^2 + \rho_n^2} - \frac{(\rho_m^2 + \rho_n^2)^2(\rho_m^2 - \rho_n^2)^2}{(2\rho_m\rho_n)^2} \\ &= \frac{d_{mn}^2}{\rho^2} - \frac{d_{mn}^2\cos^2\varphi}{\rho^2} \approx \frac{d_{mn}^2\sin^2\varphi}{\rho^2}, \end{aligned} \tag{44}$$

and

$$\begin{aligned} G(\mathcal{N}) &\approx \frac{\sum_{m=1}^{N} \frac{1}{\rho^2}}{\sum_{m=1}^{N} \sum_{n=1}^{N} \frac{d_{mn}^2 \sin^2\varphi}{\rho^2} \frac{1}{\rho^2} \frac{1}{\rho^2}}. \\ &= \frac{N\rho^4}{\sum_{m=1}^{N} \sum_{n=1}^{N} d_{mn}^2 sin^2\varphi} \end{aligned} \tag{45}$$

In the triple-antenna system such as the Intel 5300 NIC that only contains three slots for antennas, according to the average value inequality.

$$\begin{aligned} \sum_{m=1}^{3} \sum_{n=1}^{3} d_{mn}^2 &= 2(d_{12}^2 + d_{23}^2 + (d_{12} + d_{23})^2) \\ &\geq 2\left(\frac{1}{2}(d_{12} + d_{23})^2 + (d_{12} + d_{23})^2\right) \\ &= 3{d_{13}}^2. \end{aligned}$$

Only the non-uniformly spaced antenna array ($d_{12} = d_{23}$) can achieve the minimum in the inequality above. This leads to the maximum of $G(\mathcal{N})$ meaning the variance of the estimated location is the greatest.

Corollary 1. *The CRB for localizing the target that is farway from the array with $\rho \gg d_{1N}$ is $\mathcal{K}\frac{6\rho^4}{N(N^2-1)d^2\sin^2\varphi}$, if the non-uniformly spaced antenna array is used.*

Theorem 3. *For a given target and an antenna array in the polar coordinates system with the target's location as the origin, the* *utility of adding a new antenna to the array for improving the localization accuracy depends on the polar angle of the new antenna.*

Proof. In the polar coordinates system, the target's position is set as the origin. The original antenna array can be expressed as $\mathcal{N}$ with $N-1$ antennas. After adding antenna N, denoted by $\mathcal{A}_N$, the array becomes $\mathcal{N} \cup \mathcal{A}_N$. The utility of the addition is evaluated by the gain can be brought to accurate location estimation: $\mathcal{F}(\mathcal{N} \cup \mathcal{A}_N) - \mathcal{F}(\mathcal{N})$.

Note that the denominator of $G(\mathcal{N})$ satisfies the Cauchy-Schwarz inequality, which is a positive value, and $\mathcal{K}$ is also a positive constant without affecting the positiveness or negativeness of the gain. To simplify the expression of $G(\mathcal{N})$, we let $A = \sum_{m=1}^{N-1} 1/\rho_m^2$, $B = \sum_{m=1}^{N-1} \sum_{n=1}^{N-1} \frac{1}{\rho_m^2} \frac{1}{\rho_n^2} \sin^2(\theta_m - \theta_n)$, C and D denotes the increment of numerator and denominator of $G(\mathcal{N})$, respectively. Thus $C = 1/\rho_N^2$ and

$$D = \sum_{m=1}^{N-1} \frac{1}{\rho_m^2 \rho_N^2} \sin^2(\theta_m - \theta_N) = C \sum_{m=1}^{N-1} \frac{1}{\rho_m^2} \sin^2(\theta_m - \theta_N),$$

where the A, B, C, D are all positive values. Then the gain

$$\begin{aligned} \mathcal{F}(\mathcal{N} \cup \mathcal{A}_N) - \mathcal{F}(\mathcal{N}) &= \mathcal{K} \frac{BC - AD}{B(B+D)} \\ &= \mathcal{K} \frac{C(B - A \sum_{m=1}^{N-1} \frac{1}{\rho_m^2} \sin^2(\theta_m - \theta_N))}{B(B+D)}. \end{aligned} \tag{46}$$

According to Eq. (46), whether the gain is positive or negative only depends on the polar angle of the newly added antenna θ_N. □

This theorem can be used in practical deployment of CSI based localization systems. New antenna should be arranged to an appropriate position, which is for the best of most frequently visited locations.

Theorem 4. *The lowest CRB of dual-antenna array localization system with the spacing distance d can be achieved if the target is in the midperpendicular of the two antennas, and is $\frac{\sqrt{2}}{4}d$ from the midpoint of the two antennas.*

Proof. When there are only two antennas, the corresponding CRB is

$$G(\mathcal{N}) = \frac{\frac{1}{\rho_1{}^2} + \frac{1}{\rho_2{}^2}}{\frac{1}{\rho_1{}^2} \frac{1}{\rho_2{}^2} \sin^2(\theta_1 - \theta_2)}. \tag{47}$$

According to the law of cosines, $G(\mathcal{N})$ can also be written as

$$G(\mathcal{N}) = \frac{\rho_1{}^2 + \rho_2{}^2}{1 - \frac{(\rho_1{}^2 + \rho_2{}^2 - d^2)^2}{4\rho_1{}^2 \rho_2{}^2}}. \tag{48}$$

Let $t = 1/(\rho_1{}^2 + \rho_2{}^2)$, then

$$G(\mathcal{N}) \geq \frac{\rho_1{}^2 + \rho_2{}^2}{1 - \frac{(\rho_1{}^2 + \rho_2{}^2 - d^2)^2}{(\rho_1{}^2 + \rho_2{}^2)^2}} = \frac{1}{2t^2 d^2 - t^3 d^4} \geq \frac{27}{32} d^2, \tag{49}$$

$iff\ \rho_1 = \rho_2 = \sqrt{\frac{1}{2t}} = \frac{\sqrt{6}}{4} d$. The distance from the center of the two antennas is $\frac{\sqrt{2}}{4} d$. Proved. □

We note that efforts have been dedicated to study influence of anchor point placement on localization performance. For example, Spirito develops a general mathematical framework to analyze distance measurements between the mobile station and multiple base transceiver stations (BTSes) in the cellular network, which theoretically interprets how locations of BTSes can impact the localization accuracy [43]; Tekdas et al. show how to find the minimum number and optimal placement of anchor points for localizing a robot in sensor networks [42]; It also shows that the placement of anchor points in the sensor network can influence the result of CRB [32], [44].

TABLE 1
Experiment Settings

Wireless Router	TP-LINK TL-WR2041N
Anchor Point	XCY-X30 N2830 + Intel 5300 NIC
Antenna	CISCO AIR-ANT5135DG-R
Software	Linux 802.11n CSI Tool
Corridor	SEIEE Building 4th floor corridor, SJTU
NLOS	SEIEE Building 1-434 lab, SJTU
Room	SEIEE Building 1-434 lab, SJTU
Open Space	Square between SEIEE Building 1 and 2, SJTU

In the works mentioned above, the geometry of anchor points and the target is evaluated by geometric dilution of precision (GDOP), which is the ratio of the change in output location and that in measured data, quantifying how errors in the measurement will affect the final state estimation.

Our work in this section focuses on how the single anchor point should be designed to help approach to the CRLB as much as possible. However, such findings could be the basis for the possible future work studying the fundamental performance in the system with multiple CSI retrievable anchor points. It can be found that Eq. (41) is similar to the GDOP expression as they are both in the fractional form, and it is more favored that the values of the both are as less as possible. In fact, GDOP and CRB are closely related to each other, and they can be the expression of each other utilizing the variance of the data measurement and location estimation as described in [32].

7 Experimental Results

This section presents numerical results of the CRB obtained and the location estimation errors observed in experiments. The numerical results for a specific location estimation scenario are dependent on the values of the CRB parameters in the scene, such as the variance of environment noise, antenna configuration and relative positions of the antenna array and the target. We compare the numerical results with the experimental ones in the same settings, so that the theories of the paper can be understood intuitively. Since the theoretical results are based on the assumption of ideal CSI measurements and perfect location estimation algorithms, which can not be realized in practice, there must be discrepancy between the theoretical performance bounds and the experimental results. However, if the trend of the experimental results is in line with that of the theoretical ones under different impacting factors, our theoretical analysis can be corroborated. The basic experiment settings are tabulated in Table 1.

7.1 Asynchronization Error Bound

We build an AP capable of retrieving CSI using Intel 5300 toolkit and conduct experiments in a hallway as shown

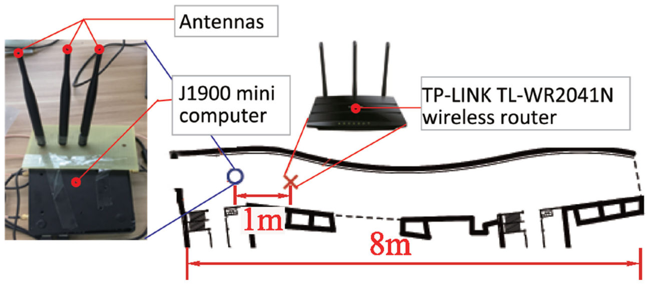

Fig. 4. Experiment environment:hallway (NLOS).

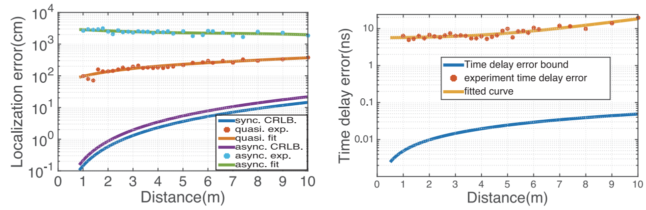

(a) Asynchronization and quasi-synchronization comparison

(b) Time delay error

Fig. 5. Asychronization error bound.

in Fig. 4. The TP-LINK TL-WR2041N wireless router is the target that sends out signals for the Intel 5300 NIC in the anchor point to catch. We implement the localization algorithm of SpotFi [18] for processing the CSI data. Intel 5300 NIC has three slots for antennas and can retrieve the CSI of 30 sub-carriers, which makes 3×30 CSI matrix available. It also provides signal to interference plus noise ratio (SINR), which can be used to estimate properties of environment noise. According to [17], [21], such CSI data are derived from the received waveform after ADC, which is in accordance with the assumptions of our theoretical analysis.

We conduct experiments to verify our asynchronization analysis in Section 6. In particular, we want to compare the localization performance with and without the asynchronization effect, and then find the time delay error bound with the synchronization mechanism.

For the synchronized case, we implement and apply the ToF sanitization algorithm in [18] to eliminate the sampling time offset (STO) in experiments, after which we can construct the smoothed matrix from the 30 subcarrier over each antenna. We further apply the improved MUSIC algorithm in [18] to the smoothed matrix. The steering vector in the MUSIC algorithm is $\vec{a}(\tau) = [1, \Omega(\tau), \ldots, \Omega^{14}(\tau)]^T$ where $\Omega(\tau) = e^{-j2\pi\Delta f\tau}$ and Δf is the frequency interval between the subcarriers. Since the sanitization algorithm is unable to eliminate the STO completely, we term the case as quasi-synchronized case. For the asynchronized case, we do not apply the sanitization algorithm, so the errors introduced by the asynchronization effect can be observed. We also plot CRLB of the two cases, where the values of the parameters are assigned based on the experiment observations.

Although not explicitly mentioned in [18], we find that the RF oscillator phase offset between antennas of the AP as observed in ArrayTrack system [20] can also occur in the Intel 5300 based system. Such phase offset is caused during the demodulation procedure, which can significantly impact the localization performance, but can be calibrated with the idea as presented in [20].

The results are shown in Fig. 5. We can see that the two curves in the lower part of Fig. 5a are CRLBs for the CSI localization system without and with synchronization, respectively. The dots in the upper part of the figure are experimental results in the two cases, where the two fitted curves based on the results are also presented. It can be seen that the theoretical bounds in the two cases are close to each other, which means that perfect precise hardware synchronization can improve the CSI localization performance in an insignificant manner. This corroborates our analysis of CRLB in Eq. (40), where it is found that the inevitable noise is the dominant factor impacting the CSI localization performance. It also can be found that the quasi-synchronization approach in [18] can indeed improve the performance in practice.

We then verify our analysis for time delay errors with the same configuration of the quasi-synchronized case as mentioned above. This is because the perfect synchronization in practice is still unavailable. We set the distance of the T-R pair from $1m$ to $10m$, and measure the corresponding ToF in each setting for 100 times. Comparing the measured ToF with the ground-truth ToF calculated with the distance divided by the speed of light, we can find the ToF estimation errors from experiments. The experimental results are compared with the theoretical error bound derived, which are illustrated in Fig. 5b. The theoretical results are obtained according to Eq. (15), where the length of DFT is 512 and the sample rate is set to be 300 MHz. This is equal to the transmitting data rate according to the 802.11n standard. The environment noise power is -95 dBm. The amplitude of the received waveform at the location that is $1m$ away from the AP is -40 dBm, and the amplitude measured in locations with different distances from the AP is basically inversely proportional to the distance according to the experiments.

As shown in Fig. 5b, we can also find the significant discrepancy between the experimental results and the theoretical error bound. Besides the inherent difference between the theory and practice, the rough ToF sanitization algorithm is another reason, which is unable to estimate accurate ToF [18]. However, we can see that the trend of the experimental results is increasing, because the farther the target is from the AP, the larger the error of estimation can be, which is in accordance with the CRLB trend. This corroborates our theoretical analysis.

7.2 Antenna Array Design

We here verify our insight into the antenna array design presented in section 6. We first examine whether the localization errors obtained with two antennas will have a greater CRLB than that with three antennas under the same circumstance. Substituting $N = 2$ into the CRLB expression, we can calculate the error bound for 2 antennas. We can construct the smoothed CSI matrix from 2 antennas CSI and obtain the location estimation with the similar method in [18]. We can see from the Fig. 6a that the theoretical bound for two antennas is greater than that for three antennas.

We next compare performance of the non-uniformly spaced antenna array with that of the uniformly spaced one. We conduct experiments with the 3-antenna anchor point, and the distances between two adjacent antennas are set as following: 1) $d_{12} = 1.5$ cm and $d_{23} = 2.5$ cm; 2) $d_{12} = 2.0$ cm and $d_{23} = 2.5$ cm; 3) $d_{12} = 2.5$ cm and $d_{23} = 2.5$ cm. The theoretical error bound are calculated with case 1) and 3).

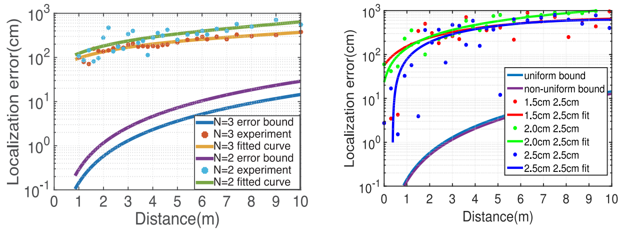

(a) Localization error with two-antenna array at 90 degree (b) Localization error with non-uniform antenna array at 90 degree

Fig. 6. Antenna array design.

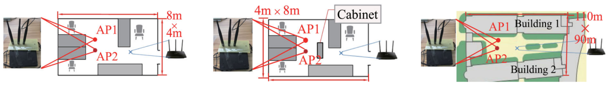

(a) Room (b) NLOS (c) Open Space

Fig. 7. Experiment environment.

The target is placed in the mid-perpendicular of the antenna array, which is moved away from the antenna array in the experiments. We run the SpotFi algorithm as in the previous experiments to estimate the target's position and then calculate the difference from the ground truth. Fig. 6b illustrates the theoretical and experimental results, from which we can see that the trends of the two kinds of results are basically complying with each other. Recall Theorem 2, the non-uniformly spaced antenna array outperforms the uniformly space one if the distance between the antennas and the target is much greater that that of the antenna array's width. We can see from Fig. 6b that the non-uniformly spaced antenna array does not outperform the uniformly spaced one when the targe is close to the anchor point, but the former outperforms the latter when the distance between the target and the anchor point is around $60 - 80$ times of the antenna array's width. When the target is more distant to the anchor point, the distance factor becomes dominant, which corroborates the theoretical results.

7.3 Practical Localization Performance

The results shown above indicate that it is reluctant to make location estimations with satisfactory accuracy using the antenna array in the single AP. This is because the ideally-strict synchronization scheme can not be realized in practice, which makes the estimated ToF unreliable; therefore, the AoA measurement results are the main basis for localization, where the data from multiple APs are more helpful for improving localization accuracy [18]. In the following experiments, we use 2 APs to localize the target in 4 kinds of environment as shown in Figs. 4 and 7. The 2-AP configuration is the basic AP deployment for examining the practical CSI localization performance.

We investigate the cases that the AP is equipped with 2 and 3 antennas, respectively. We set the midpoint between the 2 APs as the origin point, and place the target on the mid-perpendicular of the line segment joining the 2 APs. We use ρ to denote the distance between the origin point and the target when examining the influence of the distance on the performance. After that, we set the origin at the target and place the 2 APs on the circle centered at the target with radius of $1.8m$. We let the APs moving along the circle simultaneously and the orientation between the target and the antenna arrays varies. In particular, the angle between the line segment joining the two APs' antenna arrays

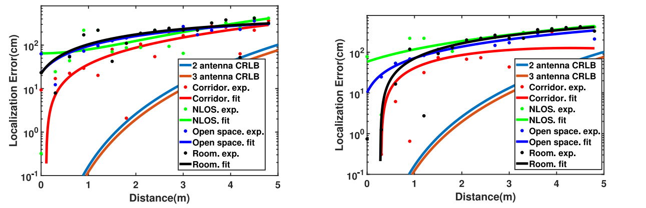

(a) Localization error with 2 antennas (b) Localization error with 3 antennas

Fig. 8. Influence of distance on localization performance.

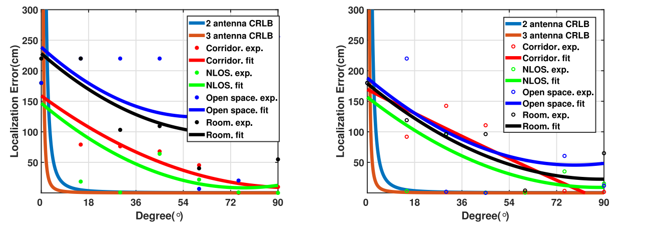

(a) Localization error with 2 antennas (b) Localization error with 3 antennas

Fig. 9. Influence of orientation on localization performance.

and the one joining the target and the AP is used to represent the orientation, which is denoted by φ.

Fig. 8 shows the influence of ρ. It can be seen that the theoretical localization errors are basically in the centimeter level, and can achieve millimeter level if ρ is around 1 meter. We perform location estimations in each of the 4 scenes for 100 times, and compare the minimum errors obtained in the experiments with the theoretical CRLBs. We can see that the trends of practical localization errors are in line with the CRLBs in all the 4 kinds of experiment environment. It shows that errors increase as the distance between the target and the origin point increases, which can be multiple meters in practical localization scenarios. We can see that the performance with 3 antennas is better than that with 2, because more antennas are helpful for accurate AoA measurements.

Note that Theorem 4 in the previous section predicts that the CRLB should reach the minimum value when the target is $\frac{\sqrt{2}}{4}d$ from the midpoint of the two antennas; therefore, it is supposed that the localization error achieves the minimum when the target is at the optimal placement and then becomes worse when deviating from the optimal position. However, such trend does not appear in Fig. 8. This is because the principle of AoA based localization approach requires the distance between adjacent antennas to be no greater than half of the wireless signal wave length [18], [20], which is less than 3 cm. That means that the target has to be placed around 1 cm from the midpoint of the two antennas, which is impractical to be verified in the experiments.

Fig. 9 shows the influence of φ. The trends of the experimental results obtained in all the 4 experiment scenes are also in line with that of the theoretical performance bounds. It can be seen that the localization errors decrease as the value of φ increases.

Fig. 10 shows more detailed experimental results to examine the influence of distance. It can be seen that the general trend of the experimental results is that the localization performance degrades as the distance between the origin and the target increases. This is in accordance with the trends as shown in Fig. 8. Fig. 11 shows the the experimental results to examine the influence of orientation. We can see

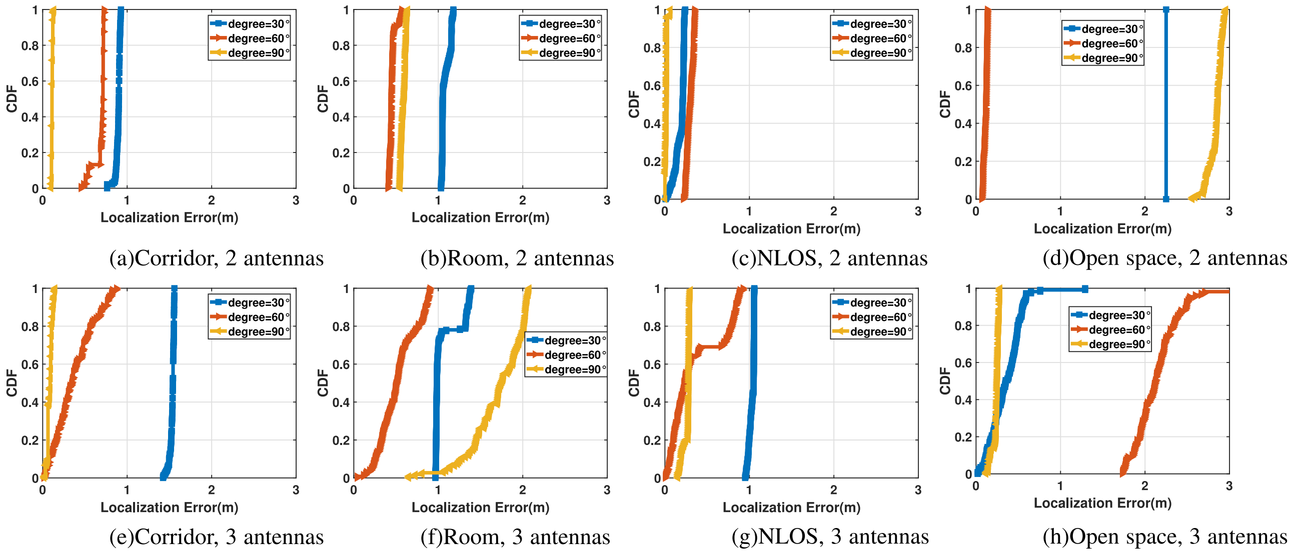

(a)Corridor, 2 antennas (b)Room, 2 antennas (c)NLOS, 2 antennas (d)Open space, 2 antennas

(e)Corridor, 3 antennas (f)Room, 3 antennas (g)NLOS, 3 antennas (h)Open space, 3 antennas

Fig. 10. Influence of degree.

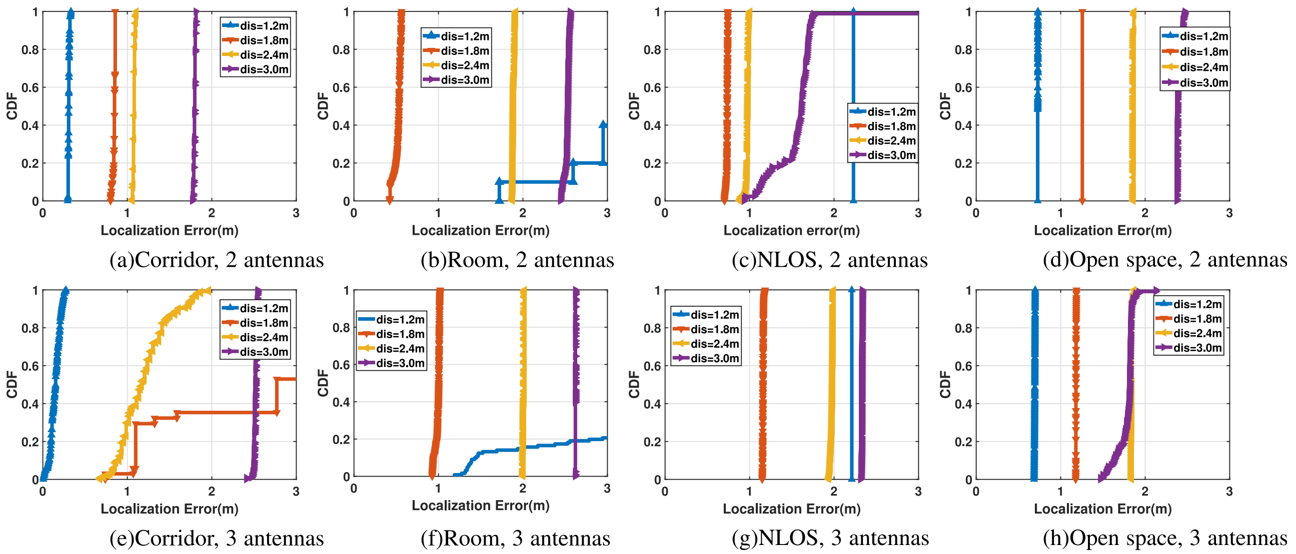

(a)Corridor, 2 antennas (b)Room, 2 antennas (c)NLOS, 2 antennas (d)Open space, 2 antennas

(e)Corridor, 3 antennas (f)Room, 3 antennas (g)NLOS, 3 antennas (h)Open space, 3 antennas

Fig. 11. Influence of distance.

that the general trend of the experimental results also corroborates that of the theoretical results. The theoretical and practical results can be references for practitioners in their system implementation process. The detailed statistics of the experimental results can be found in [45].

8 Conclusion

In this paper, we have presented an information-theoretical analysis of CSI based indoor localization approach in the received waveform level. In particular, we have derived the Cramér-Rao bound (CRB) for location estimation with the CSI approach, based on a practical signal model in accordance with Intel 5300 toolkit. We have presented a frequency domain analysis to theoretically interpret the constraining of multipath effect in practical systems and resolved the high-rank Fisher information matrix issue. Our theoretical findings have revealed insight into the design of CSI based localization systems, which shows that the sampling times for the CSI, the distribution of the target to be localized and the antenna array could fundamentally influence the localization performance. Comprehensive experimental results are demonstrated to validate our theoretical analysis.

Acknowledgments

The work in this paper is supported by the National Key Research and Development Program of China 2017YFB1003000, and the National Natural Science Foundation of China (No. 61872233, 61572319, 61829201, 61532012, 61325012, 61428205).

References

[1] K. Pahlavan, P. Krishnamurthy, and Y. Geng, "Localization challenges for the emergence of the smart world," *IEEE Access*, vol. 3, pp. 3058–3067, Dec. 2015.

[2] R. Want, A. Hopper, V. Falcao, and J. Gibbons, "The active badge location system," *ACM Trans. Inf. Syst.*, vol. 10, no. 1, pp. 91–102, 1992.

[3] A. Ward, A. Jones, and A. Hopper, "A new location technique for the active office," *IEEE Pers. Commun.*, vol. 4, no. 5, pp. 42–47, Oct. 1997.

[4] N. B. Priyantha, A. Chakraborty, and H. Balakrishnan, "The cricket location-support system," in *Proc. ACM 6th Annu. Int. Conf. Mobile Comput. Netw.*, 2000, pp. 32–43.

[5] T. S. Rappaport, et al., *Wireless Communications: Principles and Practice*. Upper Saddle River, NJ, USA: Prentice Hall, 1996, vol. 2.

[6] Y. Gwon and R. Jain, "Error characteristics and calibration-free techniques for wireless LAN-based location estimation," in *Proc. ACM. 2nd Int. Workshop Mobility Manage. Wireless Access Protocols*, 2004, pp. 2–9.

[7] H. Lim, L.-C. Kung, J. Hou, and H. Luo, "Zero-configuration, robust indoor localization: Theory and experimentation," in *Proc. 25th IEEE Int. Conf. Comput. Commun.*, 2006, pp. 1–12.

[8] K. Chintalapudi, A. Padmanabha Iyer, and V. N. Padmanabhan, "Indoor localization without the pain," in *Proc. ACM 16th Annu. Int. Conf. Mobile Comput. Netw.*, 2010, pp. 173–184.

[9] P. Bahl and V. N. Padmanabhan, "RADAR: An in-building RF-based user location and tracking system," in *Proc. 19th Annu. Joint Conf. IEEE Comput. Commun. Societies*, 2000, pp. 775–784.

[10] P. Bahl, V. N. Padmanabhan, and A. Balachandran, "Enhancements to the radar user location and tracking system," Microsoft Research, Redmond, WA, USA, Tech. Rep. MSR-TR-2000–12, 2000.

[11] T. Roos, P. Myllymäki, H. Tirri, P. Misikangas, and J. Sievänen, "A probabilistic approach to WLAN user location estimation," *Int. J. Wireless Inf. Netw.*, vol. 9, no. 3, pp. 155–164, 2002.

[12] A. Smailagic and D. Kogan, "Location sensing and privacy in a context-aware computing environment," *IEEE Wireless Commun.*, vol. 9, no. 5, pp. 10–17, Oct. 2002.

[13] A. Rai, K. K. Chintalapudi, V. N. Padmanabhan, and R. Sen, "Zee: Zero-effort crowdsourcing for indoor localization," in *Proc. ACM 18th Annu. Int. Conf. Mobile Comput. Netw.*, 2012, pp. 293–304.

[14] K. Dong, W. Wu, H. Ye, M. Yang, Z. Ling, and W. Yu, "Canoe: An autonomous infrastructure-free indoor navigation system," *Sensors*, vol. 17, no. 5, Apr. 2017, Art. no. 996.

[15] D. Vasisht, S. Kumar, and D. Katabi, "Decimeter-level localization with a single wifi access point," in *Proc. 13th Usenix Conf. Netw. Syst. Design Implementation*, 2016, pp. 165–178.

[16] IEEE 802.11 Working Group, et al., "IEEE standard for information technology–telecommunications and information exchange between systems–local and metropolitan area networks–specific requirements–part 11: Wireless LAN medium access control (mac) and physical layer (phy) specifications amendment 6: Wireless access in vehicular environments," *IEEE Std.*, vol. 802, 2010, Art. no. 11p.

[17] D. Halperin, W. Hu, A. Sheth, and D. Wetherall, "Predictable 802.11 packet delivery from wireless channel measurements," in *Proc. ACM SIGCOMM Conf.*, 2010, pp. 159–170.

[18] M. Kotaru, K. Joshi, D. Bharadia, and S. Katti, "Spotfi: Decimeter level localization using wifi," in *Proc. ACM SIGCOMM Conf.*, 2015, pp. 269–282.

[19] S. Kumar, S. Gil, D. Katabi, and D. Rus, "Accurate indoor localization with zero start-up cost," in *Proc. ACM 20th Annu. Int. Conf. Mobile Comput. Netw.*, 2014, pp. 483–494.

[20] J. Xiong and K. Jamieson, "Arraytrack: A fine-grained indoor location system," in *Proc. 10th USENIX Conf. Netw. Syst. Design Implementation*, 2013, pp. 71–84.

[21] D. Halperin, W. Hu, A. Sheth, and D. Wetherall, "Tool release: Gathering 802.11 n traces with channel state information," in *Proc. ACM SIGCOMM Conf.*, 2011, pp. 53–53.

[22] K. Kaemarungsi and P. Krishnamurthy, "Modeling of indoor positioning systems based on location fingerprinting," in *Proc. IEEE INFOCOM Conf.*, 2004, pp. 1012–1022.

[23] E. Elnahrawy, X. Li, and R. P. Martin, "The limits of localization using signal strength: A comparative study," in *Proc. 1st Annu. IEEE Commun. Soc. Conf. Sensor Ad Hoc Commun. Netw.*, 2004, pp. 406–414.

[24] G. Chandrasekaran, M. A. Ergin, J. Yang, S. Liu, Y. Chen, M. Gruteser, and R. P. Martin, "Empirical evaluation of the limits on localization using signal strength," in *Proc. 6th Annu. IEEE Commun. Soc. Conf. Sensor Mesh Ad Hoc Commun. Netw.*, 2009, pp. 1–9.

[25] H. Liu, J. Yang, S. Sidhom, Y. Wang, Y. Chen, and F. Ye, "Accurate wifi based localization for smartphones using peer assistance," *IEEE Trans. Mobile Comput.*, vol. 13, no. 10, pp. 2199–2214, Oct. 2014.

[26] H. Liu, Y. Gan, J. Yang, S. Sidhom, Y. Wang, Y. Chen and F. Ye, "Push the limit of WiFi based localization for smartphones," in *Proc. ACM 18th Annu. Int. Conf. Mobile Comput. Netw.*, 2012, pp. 305–316.

[27] R. Schmidt, "Multiple emitter location and signal parameter estimation," *IEEE Trans. Antennas Propag*, vol. 34, no. 3, pp. 276–280, Mar. 1986.

[28] Z. Yang, Z. Zhou, and Y. Liu, "From RSSI to CSI: Indoor localization via channel response," *ACM Comput. Surv.*, vol. 46, no. 2, pp. 1–32, 2013.

[29] S. M. Kay, "Fundamentals of Statistical Signal Processing: Estimation Theory," Englewood Cliffs, NJ, USA: Prentice-Hall, 1993.

[30] Y. Wen, X. Tian, X. Wang, and S. Lu, "Fundamental limits of RSS fingerprinting based indoor localization," in *Proc. IEEE Conf. Comput. Commun. (INFOCOM)*, 2015, pp. 2479–2487.

[31] Y. Geng and K. Pahlavan, "Design, implementation, and fundamental limits of image and RF based wireless capsule endoscopy hybrid localization," *IEEE Trans. Mobile Comput*, vol. 15, no. 8, pp. 1951–1964, Aug. 2016.

[32] N. Patwari, J. N. Ash, S. Kyperountas, A. O. Hero, R. L. Moses, and N. S. Correal, "Locating the nodes: Cooperative localization in wireless sensor networks," *IEEE Signal Process. Mag*, vol. 22, no. 4, pp. 54–69, Jul. 2005.

[33] N. Patwari, A. O. Hero, M. Perkins, N. S. Correal, and R. J. O'dea, "Relative location estimation in wireless sensor networks," *IEEE Trans. Signal Process*, vol. 51, no. 8, pp. 2137–2148, Aug. 2003.

[34] M. Angjelichinoski, D. Denkovski, V. Atanasovski, and L. Gavrilovska, "Cramér–rao lower bounds of RSS-based localization with anchor position uncertainty," *IEEE Trans. Inf. Theory*, vol. 61, no. 5, pp. 2807–2834, May 2015.

[35] Y. Shen and M. Z. Win, "Fundamental limits of wideband localization part I: A general framework," *IEEE Trans. Inf. Theory*, vol. 56, no. 10, pp. 4956–4980, Oct. 2010.

[36] A. M. Hossain and W. S. Soh, "Cramer-RAO bound analysis of localization using signal strength difference as location fingerprint," in *Proc. IEEE INFOCOM*, 2010, pp. 1–9.

[37] J. Xiong, K. Sundaresan, and K. Jamieson, "Tonetrack: Leveraging frequency-agile radios for time-based indoor wireless localization," in *Proc. ACM 21st Annu. Int. Conf. Mobile Comput. Netw.*, 2015, pp. 537–549.

[38] H. Liu, Y. Gan, J. Yang, S. Sidhom, Y. Wang, Y. Chen, and F. Ye, "Push the limit of wifi based localization for smartphones," in *Proc. ACM 18th Annu. Int. Conf. Mobile Comput. Netw.*, 2012, pp. 305–316.

[39] Y. Xie, Z. Li, and M. Li, "Precise power delay profiling with commodity WiFi," in *Proc. ACM 21st Annu. Int. Conf. Mobile Comput. Netw.*, 2015, pp. 53–64.

[40] Warp project. (2017). [Online]. Available: http://warpproject.org

[41] Atheros CSI Tool. (2017). [Online]. Available: http://pdcc.ntu.edu.sg/wands/Atheros/#cite

[42] O. Tekdas and V. Isler, "Sensor placement for triangulation-based localization," *IEEE Trans. Autom. Sci. Eng.*, vol. 7, no. 3, pp. 681–685, Jul. 2010.

[43] M. A. Spirito, "On the accuracy of cellular mobile station location estimation," *IEEE Trans. Veh. Technol.*, vol. 50, no. 3, pp. 674–685, May 2001.

[44] N. Salman, H. K. Maheshwari, A. H. Kemp, and M. Ghogho, "Effects of anchor placement on mean-CRB for localization," in *Proc. 10th IFIP Annu. Mediterranean Ad Hoc Netw. Workshop*, 2011, pp. 115–118.

[45] Statistics of CSI localization experiments. (2018). [Online]. Available: https://www.dropbox.com/s/0aect8y9m1pzkae/CSI-Exp

Xiaohua Tian (S'07-M'11) received the BE and ME degrees in communication engineering from Northwestern Polytechnical University, Xian, China, in 2003 and 2006, respectively, and the PhD degree in the Department of Electrical and Computer Engineering (ECE), Illinois Institute of Technology (IIT), Chicago, in Dec. 2010. Since Mar. 2011, he has been with the School of Electronic Information and Electrical Engineering at Shanghai Jiao Tong University, and now is an associate professor with the title of SMC-B scholar. He serves as the column editor of the *IEEE Network Magazine* and the guest editor of the *International Journal of Sensor Networks* (2012). He also serves as the TPC member for IEEE INFOCOM 2014-2017, a best demo/poster award committee member of IEEE INFOCOM 2014, the TPC co-chair for IEEE ICCC 2014-2016, the TPC co-chair for the 9th International Conference on Wireless Algorithms, Systems and Applications (WASA 2014), a TPC member for IEEE GLOBECOM 2011-2016, and TPC member for IEEE ICC 2013-2016, respectively. He is a member of the IEEE.

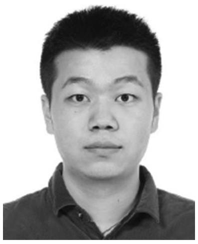

Sujie Zhu received the BE degree in information engineering from Shanghai Jiao Tong University, in 2017. His research interests include Internet of Things(IOT) including indoor localization and smart wearable devices.

Sijie Xiong received the BE degree in information engineering from Shanghai Jiao Tong University, in 2017. His recent research interests include mobile network and system.

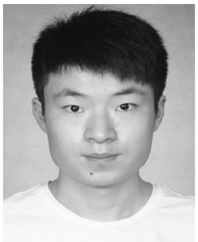

Binyao Jiang is currently working toward the BE degree in computer science from Shanghai Jiao Tong University, China, and is expected to graduate in 2019. His recent research work is on indoor localization.

Yucheng Yang is currently working toward the BE degree in electronics engineering from Shanghai Jiao Tong University, China and is expected to graduate in 2017. His recent research work is on indoor localization.

Xinbing Wang received the BS degree (with hons.) from the Department of Automation, Shanghai Jiaotong University, Shanghai, China, in 1998, the MS degree from the Department of Computer Science and Technology, Tsinghua University, Beijing, China, in 2001, and the PhD degree, major from the Department of Electrical and Computer Engineering, minor in the Department of Mathematics, North Carolina State University, Raleigh, in 2006. Currently, he is a professor with the Department of Electronic Engineering, Shanghai Jiaotong University, Shanghai, China. He has been an associate editor for the *IEEE/ACM Transactions on Networking* and the *IEEE Transactions on Mobile Computing*, and the member of the Technical Program Committees of several conferences including ACM MobiCom 2012, ACM MobiHoc 2012-2014, and IEEE INFOCOM 2009-2017. He is a senior member of the IEEE.